doi:10.1093/brain/awu067 Brain 2014: 137; 1361–1373 | 1361

BRAIN
A JOURNAL OF NEUROLOGY

PRKAR1B mutation associated with a new neurodegenerative disorder with unique pathology

Tsz Hang Wong,[1,*] Wang Zheng Chiu,[1,*] Guido J. Breedveld,[2] Ka Wan Li,[3] Annemieke J. M. H. Verkerk,[4] David Hondius,[3,5] Renate K. Hukema,[2] Harro Seelaar,[1] Petra Frick,[6] Lies-Anne Severijnen,[2] Gert-Jan Lammers,[7] Joyce H. G. Lebbink,[8] Sjoerd G. van Duinen,[9] Wouter Kamphorst,[5] Annemieke J. Rozemuller,[5] Netherlands Brain Bank,[10] E. Bert Bakker,[11] The International Parkinsonism Genetics Network[§], Manuela Neumann,[6,12] Rob Willemsen,[2] Vincenzo Bonifati,[2] August B. Smit[3] and John van Swieten[1,13,14]

1 Department of Neurology, Erasmus Medical Centre, 3015 CE Rotterdam, The Netherlands
2 Department of Clinical Genetics, Erasmus Medical Centre, 3015 CE Rotterdam, The Netherlands
3 Department of Molecular and Cellular Neurobiology, Centre for Neurogenomics and Cognitive Research, Neuroscience Campus Amsterdam, VU University, 1081 HV Amsterdam, The Netherlands
4 Department of Internal Medicine, Erasmus Medical Centre, 3015 CE Rotterdam, The Netherlands
5 Department of Pathology, VU University Medical Centre, De Boelelaan 1117, 1081 HV Amsterdam, The Netherlands
6 DZNE, German Centre for Neurodegenerative Disease, 72076 Tübingen, Germany
7 Department of Neurology, Leiden University Medical Centre, 2300 RC Leiden, The Netherlands
8 Department of Cell Biology and Genetics and Department of Radiation Oncology, Erasmus Medical Centre, 3015 CE Rotterdam, The Netherlands
9 Department of Pathology, Leiden University Medical Centre, 2300 RC Leiden, The Netherlands
10 Netherlands Institute for Neuroscience, Meibergdreef 47, 1105 BA Amsterdam, The Netherlands
11 Department of Clinical Genetics, Leiden University Medical Centre, 2300 RC Leiden, The Netherlands
12 Department of Neuropathology, University of Tübingen, 72076 Tübingen, Germany
13 Alzheimer Centre, Neuroscience Campus Amsterdam, 1007 MB Amsterdam, The Netherlands
14 Department of Neurology, Neuroscience Campus Amsterdam, 1007 MB Amsterdam, The Netherlands

*These authors contributed equally to this work.
[§]A list of contributors can be found in Appendix 1.

Correspondence to: Prof. John C. van Swieten, MD, PhD,
Department of Neurology, Erasmus Medical Centre Rotterdam,
Room Hs 611, 's-Gravendijkwal 230,
3015 CE Rotterdam, The Netherlands
E-mail: j.c.vanswieten@erasmusmc.nl

Pathological accumulation of intermediate filaments can be observed in neurodegenerative disorders, such as Alzheimer's disease, frontotemporal dementia and Parkinson's disease, and is also characteristic of neuronal intermediate filament inclusion disease. Intermediate filaments type IV include three neurofilament proteins (light, medium and heavy molecular weight neurofilament subunits) and α-internexin. The phosphorylation of intermediate filament proteins contributes to axonal growth, and is regulated by protein kinase A. Here we describe a family with a novel late-onset neurodegenerative disorder presenting with dementia and/or parkinsonism in 12 affected individuals. The disorder is characterized by a unique neuropathological phenotype displaying abundant neuronal inclusions by haematoxylin and eosin staining throughout the brain with immunoreactivity for intermediate filaments. Combining linkage analysis, exome sequencing and proteomics analysis, we identified a heterozygous c.149T>G (p.Leu50Arg) missense mutation in the gene encoding the protein kinase A type I-beta regulatory subunit (*PRKAR1B*). The pathogenicity of the mutation is supported by segregation in the family, absence in variant

Received October 1, 2013. Revised December 13, 2013. Accepted January 28, 2014

databases, and the specific accumulation of PRKAR1B in the inclusions in our cases associated with a specific biochemical pattern of PRKAR1B. Screening of *PRKAR1B* in 138 patients with Parkinson's disease and 56 patients with frontotemporal dementia did not identify additional novel pathogenic mutations. Our findings link a pathogenic *PRKAR1B* mutation to a novel hereditary neurodegenerative disorder and suggest an altered protein kinase A function through a reduced binding of the regulatory subunit to the A-kinase anchoring protein and the catalytic subunit of protein kinase A, which might result in subcellular dislocalization of the catalytic subunit and hyperphosphorylation of intermediate filaments.

Keywords: intermediate filament; neurofilament; protein kinase A; neurodegenerative disorders; *PRKAR1B*

Abbreviations: AKAP = A-kinase anchoring protein; D/D = dimerization/docking; FTD = frontotemporal dementia; FTLD = frontotemporal lobar degeneration; NIFID = neuronal intermediate filament inclusion disease; PKA = protein kinase A; SNP = single nucleotide polymorphism

Introduction

Neurofilament proteins assembling into neuron-specific intermediate filaments type IV, are major constituents of the axonal cytoskeleton. Neurofilaments undergo significant changes in their subunit composition during development and in adult neurons, and play an essential role in axonal growth, axonal transport and signalling pathways (Szaro and Strong, 2010). In the CNS, the major neuronal intermediate filaments can be distinguished into three neurofilaments proteins: NF-L (light), NF-M (medium) and NF-H (heavy), and α-internexin, each composed of an N-terminal head domain, an α-helix-rich central rod domain, and a C-terminal tail domain (Lariviere and Julien, 2004). Phosphorylation of the Lys-Ser-Pro repeat sites at the C-tail of NF-H and NF-M and at sites at the N-terminal domain, was proven to be essential for neurofilament-specific function (Rao *et al.*, 2012). The cyclic AMP-dependent protein kinase A (PKA) plays a major role in phosphorylation of neurofilaments (Sihag *et al.*, 1999), and hyperphosphorylation of Lys-Ser-Pro repeat sites causes disrupted neurofilament axonal transport, prevents turnover of neurofilaments by the ubiquitin proteasome system, and results in the accumulation of neurofilaments (Sihag *et al.*, 1999; Zheng *et al.*, 2003; Dale and Garcia, 2012; Holmgren *et al.*, 2012).

PKA is a heterotetramer, consisting of two regulatory and two catalytic subunits, which is inactive in the absence of cyclic AMP (Skalhegg and Tasken, 2000). Binding of cyclic AMP to regulatory subunits unleashes the catalytic subunit, thereby enabling PKA signalling. The regulatory subunits also provide binding sites for A-kinase anchoring protein (AKAP), a scaffold protein for targeting PKA signalling (Burgers *et al.*, 2012; Taylor *et al.*, 2012). Mutations in these regulatory subunits have been shown to alter PKA function (Burton *et al.*, 1997; Greene *et al.*, 2008).

Several neurodegenerative disorders, such as Alzheimer's disease, Parkinson's disease, motor neuron disease, and frontotemporal dementia (FTD) show aggregation of neurofilaments in association with disease-specific accumulation of tau, α-synuclein or transactive response DNA-binding protein 43 (TARDBP, previously known as TDP-43), respectively (Dale and Garcia, 2012). Neuronal intermediate filament inclusion disease (NIFID), a rare neurodegenerative disorder, shows neurofilament and fused in sarcoma (FUS) protein-positive inclusions, which are negative for tau, TARDBP and α-synuclein (Josephs *et al.*, 2003; Cairns *et al.*, 2004*b*, *c*, 2007; Uchikado *et al.*, 2005; Neumann *et al.*, 2009). NIFID is a non-familial disorder (Josephs *et al.*, 2003; Cairns *et al.*, 2004*a*; Molina-Porcel *et al.*, 2008), and neither pathogenic variants in any of the genes coding for intermediate filaments and FUS, nor biochemical modifications of intermediate filaments were found (Cairns *et al.*, 2004*c*; Momeni *et al.*, 2006; Dequen *et al.*, 2011).

Furthermore, neurofilament inclusions are found in patients with Charcot–Marie–Tooth disease type 2E and in transgenic mice with a mutation at the major phosphorylation site (Ser55Asp) of the *Nefl* gene (Gibb *et al.*, 1998; Fabrizi *et al.*, 2004; Sasaki *et al.*, 2006). Also, a transgenic mouse model overexpressing α-internexin, induces the formation of cerebellar torpedoes, and abnormal accumulation of neuronal intermediate filaments (Ching *et al.*, 1999).

In this paper, we report a novel familial neurodegenerative disorder with a highly specific neuropathological phenotype consisting of abundant α-internexin-positive, but FUS-negative neuronal inclusions. By means of genome-wide linkage analysis, exome sequencing and proteomics of neuronal inclusions, we have identified a pathogenic mutation in the gene coding for the type I-beta regulatory subunit of protein kinase A, *PRKAR1B*. The mutant protein is found to be associated with aggregates of intermediate filaments in this disease.

Materials and methods

Subjects

We studied a three generation-large family with 12 affected patients presenting with dementia and/or extrapyramidal syndrome (Fig. 1 and Table 1). Medical information was limited in the five deceased affected members (Patients II:1, III:1, III:12, III:13 and III:14). One clinically unaffected patient, Patient III:9, who died from myeloid leukaemia at 57 years old, has been described with α-synuclein negative Lewy bodies previously (van Duinen *et al.*, 1999). The proband (Patient III:4) from this family was evaluated for motor and mental complaints at the age of 56 years. The age at onset of the affected individuals varied between 45 and 64 years, the mean disease duration was 14.8 years, but varied from 5 to 25 years.

DNA was extracted from peripheral blood samples of Patients III:2, III:3, III:4, III:5, III:6, III:10 and III:11, and from the spleen of Patient III:9. The study was approved by the Medical Ethical Committee of the

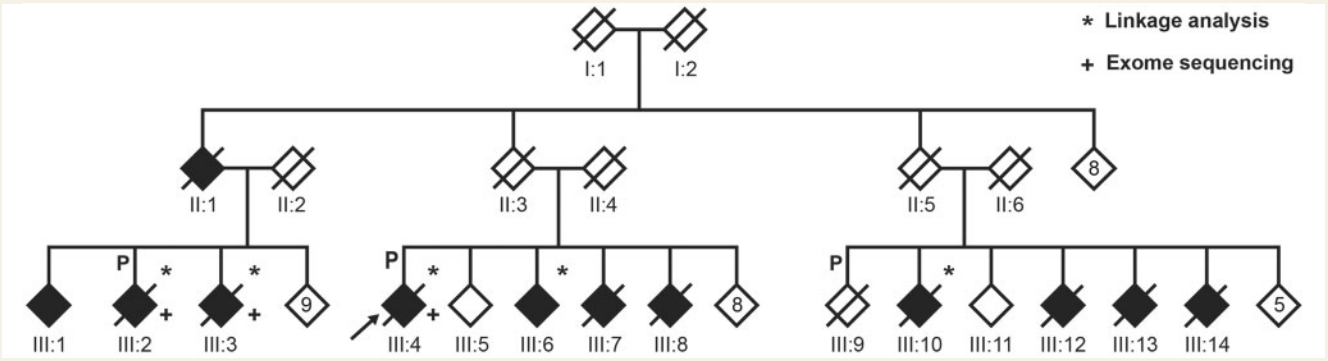

Figure 1 Pedigree of the family with *PRKAR1B* mutation. Filled symbols represent affected individuals by behavioural symptoms, dementia and or parkinsonism, and empty symbols represent unaffected individuals. Symbols with a diagonal line represent deceased individuals. Pathology is denoted by P, and the proband is indicated by arrow. Numbers in symbols indicates the number of individuals. Sex of the pedigree members are obscured to protect privacy. * = individuals included in linkage analysis; + = individuals included in exome sequencing.

Table 1 Clinical characteristics of the individuals in the family

Patient	Age at onset	Age at death	Duration	Current age	Dementia	Parkinsonism	Atrophy on MRI/CT
II:1	45	70	25	-	+	+	NA
III:1	NA	NA	NA	NA	-	+	NA
III:2[a]	50	67	17	-	+	_	NA
III:3	50	75	25	-	+	NA	Frontal
III:4[a]	56	61	5	-	+	+	Generalized
III:5	-	-	-	65	-	-	NA
III:6	60	-	-	67	+	+	Generalized
III:7	<57	63	NA	-	+	NA	NA
III:8	<60	62	NA	-	+	NA	NA
III:9[a]	-	57	-	-	-	-	NA
III:10	63	71	8	-	+	+	Generalized
III:11	-	-	-	80	-	-	NA
III:12	<65	67	NA	-	+	NA	NA
III:13	64	73	9	-	+	NA	Generalized
III:14	NA	74	NA	-	+	NA	NA
Range	45–64	61–75	5–25				

+ or – indicate the presence or absence of the phenotype or information; NA = not available.
[a]Autopsy confirmed cases.

Erasmus Medical Centre Rotterdam, and all family members participating in the study or their legal representatives gave informed consent. A series of 138 unrelated patients with Parkinson's disease and an autosomal dominant pattern of inheritance were also studied. The clinical diagnosis of Parkinson's disease was established according to widely used criteria (Hughes *et al.*, 1992). The patients originated from Italy ($n = 114$), Brazil ($n = 14$), Portugal ($n = 9$) and The Netherlands ($n = 1$). The average onset age of Parkinson's disease symptoms was 53.5 ± 11.7 years (range 20–75 years), and the average disease duration was 8.5 ± 7.1 years (range 1–36 years). In these patients the entire *PRKAR1B* coding region (10 exons) and exon–intron boundaries were sequenced by Sanger protocols to find possible pathogenic variants. Primers and PCR protocols are reported in Supplementary Table 1. *PRKAR1B* variants were also analysed in exome sequenced cohorts of familial FTD ($n = 51$) and FTD-FUS ($n = 5$). The average onset age of symptoms was 58.4 ± 8.6 years (range 36–73 years) in familial FTD and 33.7 ± 2.4 years (range 30–36 years) in FTD-FUS. The average disease duration was 66.8 ± 8.8 years (range 43–83 years) in familial FTD and 43.1 ± 3.7 years (range 39–46 years) in FTD-FUS.

Genomic analysis

CSV files containing single nucleotide polymorphism (SNP) call data from HumanCytoSNP-12v2.1(Illumina) arrays of five related patients (Fig. 1) were adapted by GenomeStudio (Illumina) for linkage analyses using Allegro (Gudbjartsson *et al.*, 2000) implemented in easyLINKAGE Plus (Hoffmann and Lindner, 2005). SNPs with a call rate <95% were excluded from the calculations. Mendelian inheritance check was performed for all family members, with the program PedCheck (O'Connell and Weeks, 1998). SNPs showing Mendelian inconsistencies were excluded from the calculation. Individuals who were encoded by the pedigree information file were used for allele

frequencies computation. Two separate multipoint linkage analyses were performed (affected only) on genotypes from five affected individuals using Allegro with a SNP spacing of 0.2 cM and one of 0.5 cM. Logarithm of the odds (LOD) scores in sets of 100 markers were calculated assuming the disease to be an autosomal dominant disorder with a gene frequency of 0.0001 in the population. Regions showing a LOD score >1.5 in both models were used as candidate regions (Supplementary Fig. 1). As borders, flanking SNP markers were used. Additionally, genome wide copy number analysis in genotyped individuals was performed using signal intensity files generated with GenomeStudio 2011, V2011.1 (Illumina) in Nexus Copy Number, Discovery Edition, ver. 5.1 (BioDiscovery).

Patients III:2, III:3 and III:4 were selected for exome sequencing (Fig. 1). Whole exome capture and sequencing were performed by LGC Genomics. Exomes were captured by Agilent's SureSelect AllExon Kit, and were sequenced with 100-bp reads on the Illumina HiSeq2000 platform, according to the manufacturer's protocol. Reads were mapped to the human reference genome sequence (assembly GRCh37/hg19) using the Burrows-Wheeler Alignment Tool (Li and Durbin, 2009). The identified variants per individual were called by using the Genome analysis Tool Kit (GATK) and annotated by ANNOVAR (McKenna *et al.*, 2010; Wang *et al.*, 2010). GATK was also used for base quality recalibration, local sequence realignment and variant filtering to minimize base calling and mapping errors. Variants with quality score <30, quality over depth <5, strand bias >-0.10 and depth <20 were filtered out. Additionally, Indels with strandbias >-1.0 instead of -0.10 were filtered out. We used the dbSNP129 (http://www.ncbi.nlm.nih.gov/projects/SNP/), the 1000 Genome Project (www.1000genomes.org/) and the National Heart Lung Blood Institute Exome Variant Server (https://evs.gs.washington.edu/EVS/) to filter out polymorphisms. The predicted functional effects of the novel sequence variants were assessed by PolyPhen2 (http://genetics.bwh.harvard.edu/pph2/), Sorting Intolerant from Tolerant (SIFT) (http://sift.jcvi.org/www/SIFT_enst_submit.html), PROVEAN (http://provean.jcvi.org/seq_submit.php) and Mutation Taster (www.mutationtaster.org). The conservation of amino acid across different species was identified by MUCLES (Edgar, 2004).

Histology and immunohistochemistry

The Netherlands Brain Bank performed brain autopsy (Patients III:2 and III:4) within 4 h of death according to their Legal and Ethical Code of Conduct of the Netherlands Brain Bank. Tissue blocks were taken from all cortical areas, hippocampus, amygdala, basal ganglia, substantia nigra, pons, medulla oblongata, cerebellum, and cervical spinal cord, and were embedded in paraffin blocks and subjected to routine staining with haematoxylin and eosin, periodic acid-Schiff reaction and silver staining. Brain autopsy and routine staining of the third case (Patient III:9) was described by van Duinen *et al.* (1999), and several regions were obtained for immunohistochemistry.

Immunohistochemistry was performed with antibodies directed against: hyperphosphorylated tau (AT-8, Innogenetics; 1:400); amyloid-β protein (Dako; 1:100, following formic acid pretreatment); α-synuclein (Zymed Laboratories; undiluted, after formic acid pretreatment); poly-ubiquitin-binding protein p62 (BD Biosciences Pharmingen; 1:200, after pressure cooking); TARDBP (ProteinTech Group; 1:100, after pressure cooking); neuroserpin (Abcam; 1:100); SMI-31 (Sternberger; 1:5000); SMI-32 (Sternberger; 1:7000) α-internexin (Invitrogen, 1:100, after pressure cooking); FUS (ProteinTech; 1:25–1:200 with initial overnight incubation at room temperature, after pressure cooking), and PRKAR1B (2× anti-PRKAR1B, Abcam ab38225; 1:50 and Santa Cruz Biotechnology SC-907, Inc; 1:125). Specificity of PRKAR1B antibody is described in other studies (Chang *et al.*, 2003; Zhang *et al.*, 2004). Primary antibodies were incubated overnight at 4°C followed with BrightVision horseradish peroxidase-linked secondary antibody (Immunologic). The immunoreactivity was visualized by freshly prepared Liquid DAB Substrate Chromogen solution (Dako). Slides were counterstained with Mayer's haematoxylin and mounted in Entellan®.

Double immunofluorescence staining

For double staining, autofluorescence of brain tissue was quenched by treatment with 0.1% Sudan Black B (Sigma-Aldrich) in 70% ethanol. Secondary antibodies were Cy3-conjugated anti-mouse (Jackson ImmunoResearch; 1:100) and Alexa Fluor® 488-conjugated anti-rabbit secondary antibody (Invitrogen; 1:100). Slides were mounted in Mowiol® and analysed by confocal microscope (Leica).

Electron microsocopy

Minute pieces of frontal cortex were fixed in 4% glutaraldehyde in 0.1 M phosphate (pH 7.2), postfixed in 1% osmium tetroxide and embedded in Epon®. Semi-thin sections (1 μm) were stained with Toluidine blue. Areas of interest were selected for ultrathin sectioning (50–60 nm). Contrast was enhanced by staining with lead citrate.

Quantitative proteomics

Approximately 1000 positive inclusions were excised by laser capture microdissection (Carl Zeiss Microscopy) from each of the two brains (Patients III:2 and III:4). In addition, tissues from the same brain areas of two healthy control brains without inclusions were collected in the same manner. Tissues were lysed in 25 μl SDS sample buffer, separated by 10% SDS PAGE, and stained with colloidal Coomassie blue. Each gel lane was cut into two gel pieces of equal size, destained, and incubated with trypsin (1 μg, Promega) for 16 h at 37°C.

Peptides were separated on a 200 mm reversed phase nano-column (100 μm ID packed with 3 μm Alltima™ C18 particle from Alltech) using an Eksigent NanoLC Ultra® system (AB-Sciex). The acetonitrile concentration in 0.1% acetic acid was increased linearly from 4.5% to 38% in 40 min, and to 80% in 1 min. The flow rate was 400 nl/min. The eluted peptides were electro-sprayed into the LTQ-Orbitrap discovery (Thermo Electron). The mass spectrometer was operated in a data-dependent mode, in which one mass spectrometry (MS) full scan (m/z range from 330 to 2000) was followed by MS/MS scans on five most abundant ions. The exclusion window was 25 s. The mass spectrometric data were searched against the IPI human database (ipi human v3.87) with MaxQuant software (version 1.3.0.5). The search parameters were MS tolerance, 20 ppm; MS/MS tolerance, 0.5 Da; enzyme, trypsin with maximum missed cleavages of 2.

Sequential biochemical fractionation and immunoblot analysis:

Post-mortem frozen brain tissue from two cases (Patients III:2 and III:4), two frontotemporal lobar degeneration (FTLD) TDP cases and two Alzheimer's disease cases, were dissected, weighted, and sequentially extracted with buffers of increasing strength as previously described (Neumann *et al.*, 2006). Briefly, grey matter was extracted at 5 ml/g (volume/weight) with low salt buffer (10 mM Tris, pH 7.5, 5 mM EDTA, 1 mM DTT, 10% sucrose, and a cocktail of

protease inhibitors), high salt-Triton buffer (low salt + 1% Triton^{TM} X-100 + 0.5 M NaCl), myelin floatation buffer (30% sucrose in low salt + 0.5 M NaCl), and sarkosyl (SARK) buffer (1% *N*-lauroyl-sarcosine in low salt + 0.5 M NaCl). The SARK insoluble material was extracted in 0.25 ml/g urea buffer {7 M urea, 2 M thiourea, 4% 3-[(3-cholamidopropyl) dimethylammonio]-1-propanesulphonate (CHAPS), 30 mM Tris, pH 8.5}. Proteins were resolved by 7.5% SDS-PAGE and transferred to PVDF membranes (Millipore).

Following transfer, membranes were blocked with Tris buffered saline containing 3% powdered milk and probed with the mouse monoclonal antibody PKA [RI] raised against the C-terminal portion (amino acids 225–381) of the type I regulatory subunit (610166, Becton Dickinson Laboratories), the polyclonal antibody PKA Iβ reg [sc-907 (c-19), Santa Cruz] and a mouse monoclonal anti-α-internexin (32-3600, Invitrogen). Primary antibodies were detected with horseradish peroxidase-conjugated anti-mouse or anti-rabbit IgG (Jackson ImmunoResearch), and signals were visualized by a chemiluminescent reaction (Millipore) and the Chemiluminescence Imager Stella 3200 (Raytest).

For dephosphorylation experiments, urea fractions were dialyzed against RIPA buffer and treated with 400 units lambda phosphatase (New England Biolabs) for 30 min at 30°C.

Results

Clinical and pathological features

Behavioural changes (self-neglect, delusions), with apathy and anxiety, and memory problems with disorientation, followed by stiffness, shuffling gait, and frequent falls without tremor were the presenting symptoms in most of the patients (Table 1). Impaired attention and concentration, and deficits in memory, language, executive and visuo-constructional functions were found in two neuropsychologically evaluated patients (Patients III:4 and III:6). Mini-Mental State Examination and Frontal Assessment Battery of the proband were 20 and 6, and 18 and 8, respectively for Patient III:6. These two patients showed mild to moderate rigidity, bradykinesia, postural instability, small-stepped gait and normal ocular movements, and no cerebellar and motor neuron disease signs at neurological examination on the first evaluation. Unified Parkinson's Disease Rating Scale of the proband showed 6 points in part I, 13 points in part II, 16 points in part III, Hoehn and Yahr grade four and Schwab and England Activities of Daily Living scale of 40%. EMG in the proband revealed no evidence for motor neuron disease, myopathy or polyneuropathy. Generalized cerebral atrophy was seen on MRI or CT of the brain in Patients III:4, III:6, III:10, III:13, and more prominent frontal atrophy in the proband (Patient III:4) (Supplementary Fig. 2). Dopaminergic medication in two patients had only a modest effect. Moreover, ^{18}F-fluorodeoxyglucose PET showed frontal hypometabolism in the proband (Supplementary Fig. 2), but a normal FP-CIT scan and normal CSF profile, which is incompatible with Parkinson's disease and Alzheimer's disease. Brain autopsy was performed in Patients III:2, III:4 and III:9.

Macroscopic examination showed mild cerebral atrophy (Patients III:2, III:4 and III:9), slightly more pronounced in the frontoparietal cortex in two. An irregular tumour, defined as glioblastoma multiforme in the right temporal lobe was found in the brain of Patient III:4 (absent on MRI 1 year earlier).

The neocortex showed normal cytoarchitecture in all three brains, with moderate neuron loss in the substantia nigra in two, and severe loss of Purkinje cells in one case. Abundant eosinophilic, periodic acid-Schiff reaction negative, cytoplasmatic neuronal inclusions with a glossy weakly stained core were observed in all neocortical regions in layers 3–6, hippocampus, substantia nigra, brainstem and spinal cord. Low to moderate numbers of inclusions were seen in the caudate nucleus, putamen, pallidum and the cerebellum (Patient III:2), and in the dentate gyrus of Patient III:9. These inclusions stained strongly with p62 and α-internexin antibodies (Fig. 2A–C), and less intense with neurofilament antibodies, such as, SMI 31 and SMI 32. Larger inclusions showed a target-like picture with a halo and a weakly stained core, whereas smaller inclusions had a more homogeneous intense staining. Immunohistochemistry was negative for FUS, α-synuclein, AT-8, amyloid-β, neuroserpin, and TARDBP. No intranuclear inclusions were seen.

Genomic and proteomic analysis

Two multipoint linkage analyses of five affected patients revealed six regions with LOD score >1.5 (Supplementary Table 2). No overlapping copy number variant was detected in affected genotyped individuals. Exome sequencing produced ~6.4 Gb of reads per sample. The average coverage of targeted region was 57×, with 74%, 72%, and 74% covered at least 20× (Supplementary Table 3). This resulted into a calling of ~48 000 allelic variants per individual after quality filtering using GATK (Supplementary Fig. 3). We examined the exome data on known FTD and Parkinson's disease genes, but no pathogenic variants in known FTD genes (*GRN*, *MAPT*, *C9orf72*, *CHMP2B*, *VCP* and *FUS*) and Parkinson's disease genes (*LRRK2*, *PARK2*, *PARK7*, *PINK1*, *SNCA*, *VPS35*, *ATP13A2*, *FBXO7*, *PANK2* and *PLA2G6*) were found.

We performed the genetic analysis in two steps. First, we filtered the exome sequencing data combining with linkage analysis to reduce the number of variants. An analysis of non-synonymous, splice-sites, stop and frameshift variants (SNPs and indels) in the six regions with LOD score >1.5 showed seven variants shared by the three patients and not annotated by dbSNP129 and having an allele frequency <1% in 1000 Genomes Project and Exome Variant Server.

Second, we combined proteomics data with the candidate variants found by genetic analysis to identify the causative gene. A total of 1000 inclusions were excised by means of microlaser dissection from fresh-frozen brain samples of Patients III:2 and III:4, and corresponding inclusion-free tissue of the same size was obtained from two control brains. The dissection was repeated once from one of the patient samples to obtain a total of three replicates. Mass spectrometry of the inclusion bodies was sufficiently sensitive to identify proteins present, but not sufficient to detect protein modifications. Quantitative proteomics analysis revealed six proteins (polyubiquitin-C, α-internexin, neurofilament light polypeptide, cAMP-dependent protein kinase regulatory subunit type I-beta, neurofilament medium polypeptide and heat shock

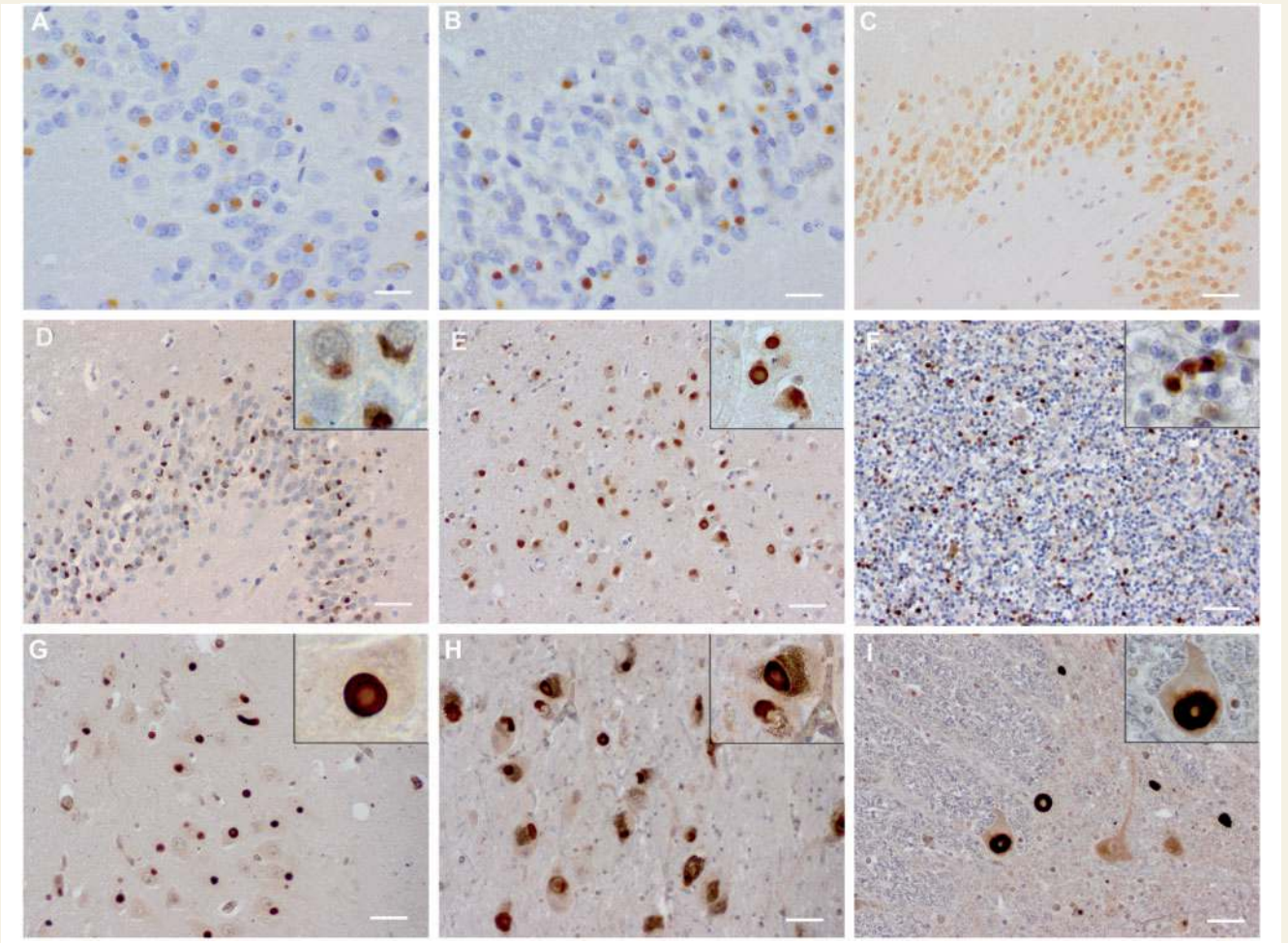

Figure 2 Distribution of neuronal cytoplasmatic inclusions found in familial neurofilamentopathy due to the mutation in the *PRKAR1B* gene. Strong immunoreactivity of neuronal cytoplasmatic inclusions with antibodies against α-internexin (**A**) and p62 (**B**) in the dentate gyrus of the hippocampus is seen in Patient III:2. Granular cells of the dentate gyrus show diffuse weak nuclear staining without cytoplasmatic inclusions with FUS antibody (**C**). PRKAR1B-positive neuronal cytoplasmatic inclusions with various sizes are abundant in the hippocampus (**D**) and frontal region (**E**). A central unstained core surrounded by a strongly immunoreactive halo is found for larger inclusions in different cortices. Many inclusions are also found in the granular layer of the cerebellum (**F**). The same finding of PRKAR1B-positive neuronal cytoplasmatic inclusions is seen in the hippocampus (**G**) of the second patient (Patient III:4). Substantia nigra show moderate neuron loss and positive immunoreactivity for PRKAR1B (**H**). These inclusions are also seen in lower motor neurons of the spinal cord (**I**). Scale bars: **A** and **B** = 20 μm; **C–I** = 50 μm.

cognate 71 kDa protein) that were present consistently and solely in the inclusion samples (Supplementary Table 4).

Combining proteomics analysis with the candidate variants from exome sequencing resulted in one single variant, the novel missense heterozygous variant in *PRKAR1B* on chromosome 7p22 (exon 2: c.149T > G; p.Leu50Arg; RefSeq NM_002735.2), which is conserved and predicted as pathogenic by four different *in silico* methods that predict functional effects of sequence variations (Fig. 3 and Supplementary Table 5). No novel and pathogenic variants were found in the genes coding for the remaining five proteins identified in the proteomics analysis of the inclusion bodies. Sanger sequencing confirmed the presence of the p.Leu50Arg variant in the affected Patients III:2, III:3, III:4, III:6, III:9 and III:10, and its absence in unaffected family members (Patients III:5 and III:11). Sequencing of the *PRKAR1B* coding region (10 exons) and exon–intron boundaries in a cohort of autosomal dominant Parkinson's disease ($n = 138$) and basophilic inclusion body disease ($n = 2$) revealed several silent and intronic polymorphisms, which are all annotated in dbSNP, and two non-synonymous rare heterozygous variants, also present in dbSNP (Supplementary Table 6). The first, p.Ile40Phe, was detected in six Parkinson's disease probands (minor allele frequency 0.013, similar to dbSNP minor allele frequency 0.022), and is considered benign by most of the prediction programs (Supplementary Table 5). The other, p.Arg232Gln, was found in only one Parkinson's disease proband, and is considered pathogenic by all the prediction programs. However, this variant does not co-segregate with Parkinson's disease in the family (one affected sib was not a carrier). This variant is also annotated in dbSNP because of just one allele detected in the 1000 Genome Project, and is not present in

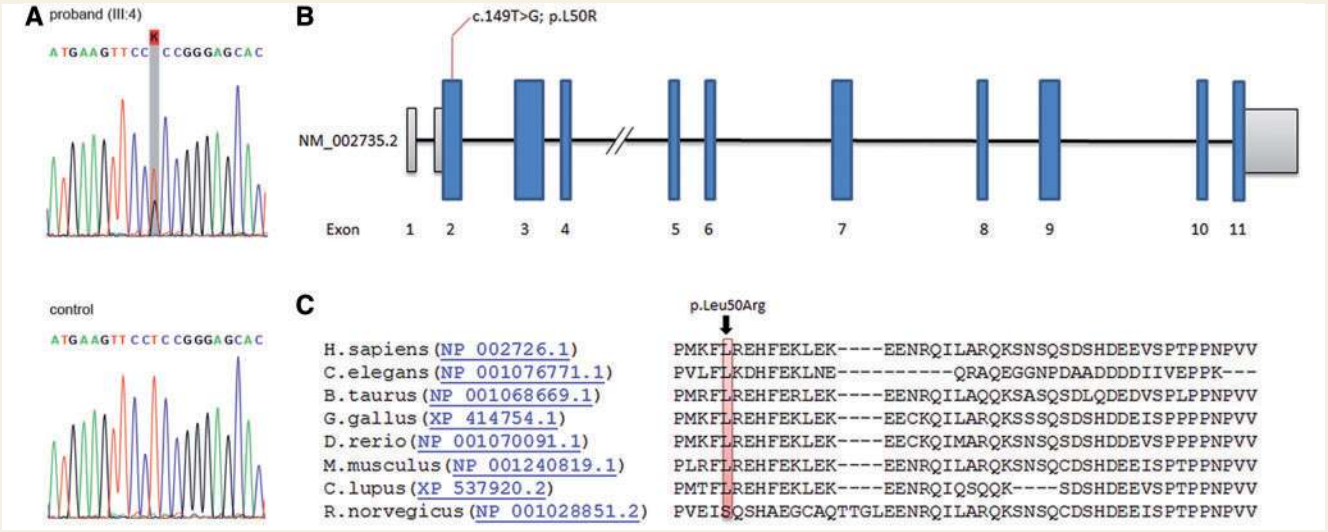

Figure 3 Schematic representation of the *PRKAR1B* genomic structure and conservation of the mutation. Electropherogram showing the *PRKAR1B* mutation at position chr7:750 997 (A > C) in exon 2 (c.T149G; p.Leu50Arg) present in the affected individual (Patient III-4) and absent in an unaffected control of the family (**A**). Schematic structure of *PRKAR1B* (isoform NM_002735.2) and the position of the mutation identified in the present study is shown. Exons are represented with blue boxes, untranslated regions in grey boxes (**B**). Alignment of the protein region containing the highly conserved leucine amino acid residue across different species is shown (**C**). The leucine at position 50 (NP_002726.1) is indicated in the red box.

the Exome Variant Server. Analysis of whole exome sequencing data in a cohort of familial FTD with unknown gene defect ($n = 51$) and FTD-FUS ($n = 5$) did not reveal any potential pathogenic rare variants in *PRKAR1B* (Supplementary Table 6).

Immunohistochemistry and biochemical analysis

Immunohistochemistry with PRKAR1B antibodies revealed intense staining of the inclusions in brain of the three cases (Fig. 2). Cytoplasmatic inclusions were exclusively seen in neurons and had a variable size. Most inclusions were round and compact with strong PRKAR1B immunoreactivity, and some neurons showed a more granular cytoplasmatic staining (Fig. 2D–I). Round inclusions were seen in the dentate granule cells (Fig. 2D), cornu ammonis 1–4, subiculum and entorhinal cortex, and in all layers of the neocortex (Fig. 2E) of Patients III:2 and III:4. Many inclusions were also observed in the hippocampus (Fig. 2G), substantia nigra (Fig. 2H), brainstem and spinal cord (Fig. 2I), whereas lower numbers of inclusions are found in the caudate nucleus, putamen and pallidum. The dentate nucleus and granular layer of the cerebellum showed many cytoplasmatic inclusions in Patient III:2 (Fig. 2F), but only some in the same region of Patient III:4. Available slices of three brain regions (pons and two neocortex) of Patient III:9 also showed abundant PRKAR1B positive inclusions. Overall, more inclusions are found in Patient III:2 than in similar regions of the other two cases. Large inclusions showed a faint core with strongly stained halo. The PRKAR1B antibody labelled the inclusions more intensely than p62 and α-internexin. No glial cytoplasmatic inclusions were seen in the cerebral white matter.

Double-labelling immunofluorescence with α-internexin and PRKAR1B antibodies showed that nearly all α-internexin positive inclusions were also PRKAR1B-positive (Fig. 4A–C). Less than five per cent of the inclusions, predominantly those with a smaller size, labelled either for α-internexin or PRKAR1B. Double labelling also showed the spatial relationship of these two proteins within the inclusions; PRKAR1B antibody often labelled the core, whereas α-internexin labelled a halo at the outer side of the inclusions (Fig. 4D–F).

Ultrastructurally, the core within the body consisted of electron-dense material, and fibrils were found in areas with remnants of vesicles and mitochondria (Fig. 4G and H). The body is composed of dense aggregates of filaments (densely packed fibrils with often a radiating aspect at the edges), whereas the paler halo consisted of bundles of both circularly and longitudinally arranged filaments.

Neurofibrillary tangles or plaques in Alzheimer's disease ($n = 4$), Lewy bodies in Parkinson's disease ($n = 10$) and Lewy body dementia ($n = 5$), glial inclusions in multiple system atrophy ($n = 4$), TARDBP-positive inclusions in FTLD ($n = 4$), Pick bodies, neurofibrillary tangles or pretangles in FTLD with *MAPT* gene mutations as well as healthy controls ($n = 4$), did not show any staining with the PRKAR1B antibody, demonstrating the specificity of PRKAR1B accumulation in our cases (data not shown).

To characterize potential biochemical alterations of PRKAR1B, proteins were sequentially extracted from temporal cortex from two cases (Patients III:2 and III:4) as well as neurological controls with a series of buffers with an increasing ability to solubilize proteins and analysed by immunoblot using an antibody that recognizes both isoforms of the type I regulatory subunits of PKA (BD Laboratories).

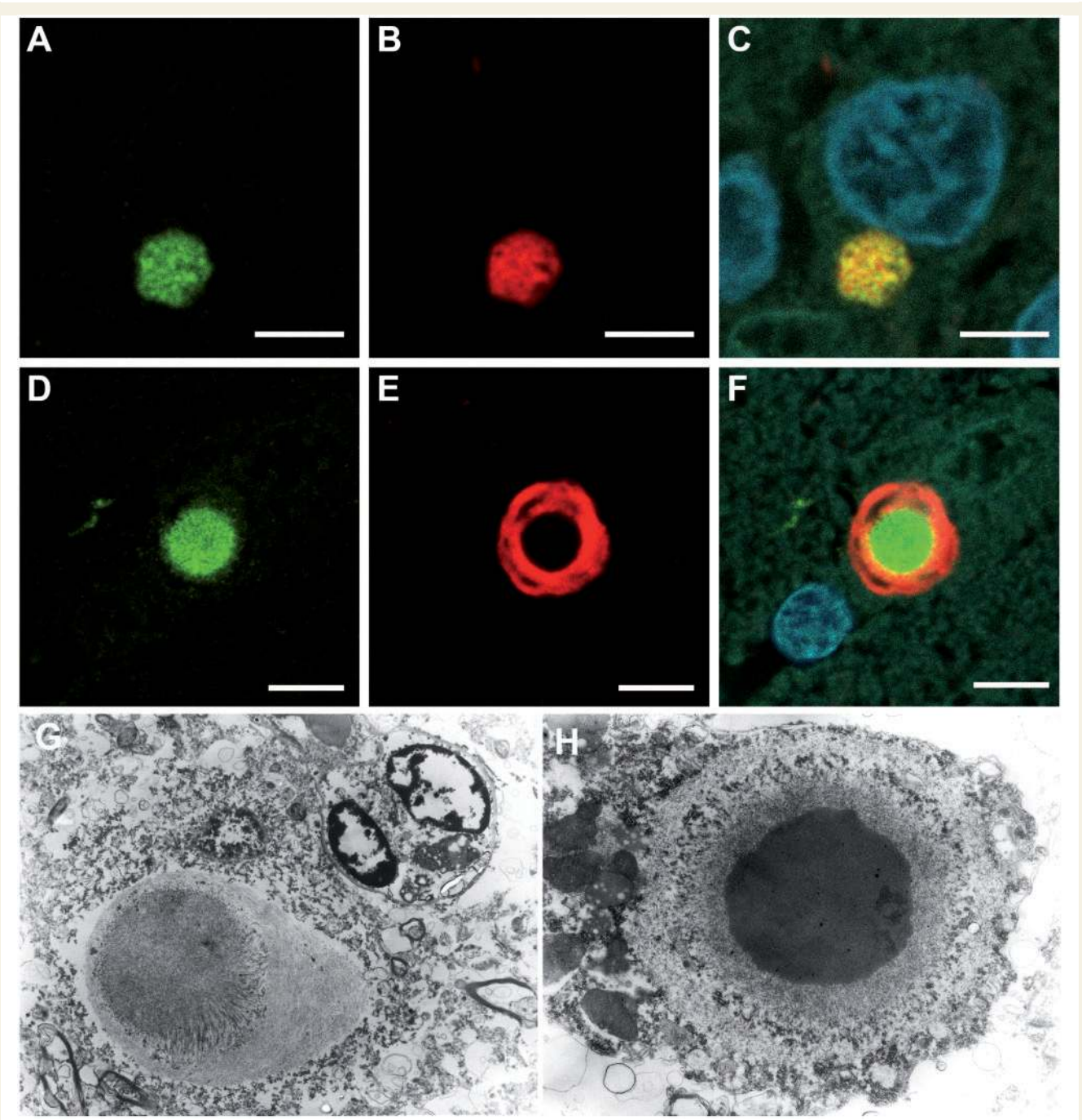

Figure 4 Double-label immunofluorescence for PRKAR1B (green) and α-internexin (red) in familial neurofilamentopathy due to *PRKAR1B* mutation. Immunofluorescence of the inclusions with PRKAR1B (**A**) and α-internexin (**B**). Some inclusions label homogeneous staining with co-localization of α-internexin and PRKAR1B (**C**). Merged images clearly show that both markers label distinct components of inclusions with a central core labelling for PRKAR1B antibody (**D**) surrounded by a halo labelling for α-internexin (**E** and **F**). Scale bars: **A** and **B** = 5 μm; **D–F** = 10 μm. (**G** and **H**) Ultrastructural examination of inclusions demonstrates dense aggregates of filaments of 11–16 nm surrounded by granule coated fibrils and cellular organelles, **G** = ×9000 and **H** = ×22 500 enlarged.

Two bands at the expected molecular weights of PRKAR1A and B (~48 and 50 kDa) were consistently present in the sarkosyl fractions in *PRKAR1B* mutation cases and FTLD and Alzheimer's disease. However, a strikingly different biochemical profile was seen in the urea fractions (fraction enriched for highly insoluble proteins) for the two *PRKAR1B* mutation cases compared with controls (Fig. 5A). Whereas controls showed only minimal reactivity in the urea fraction, a massive enrichment for PRKAR1B was observed in the two cases accompanied by the presence of additional bands of lower and higher molecular weight as well as a

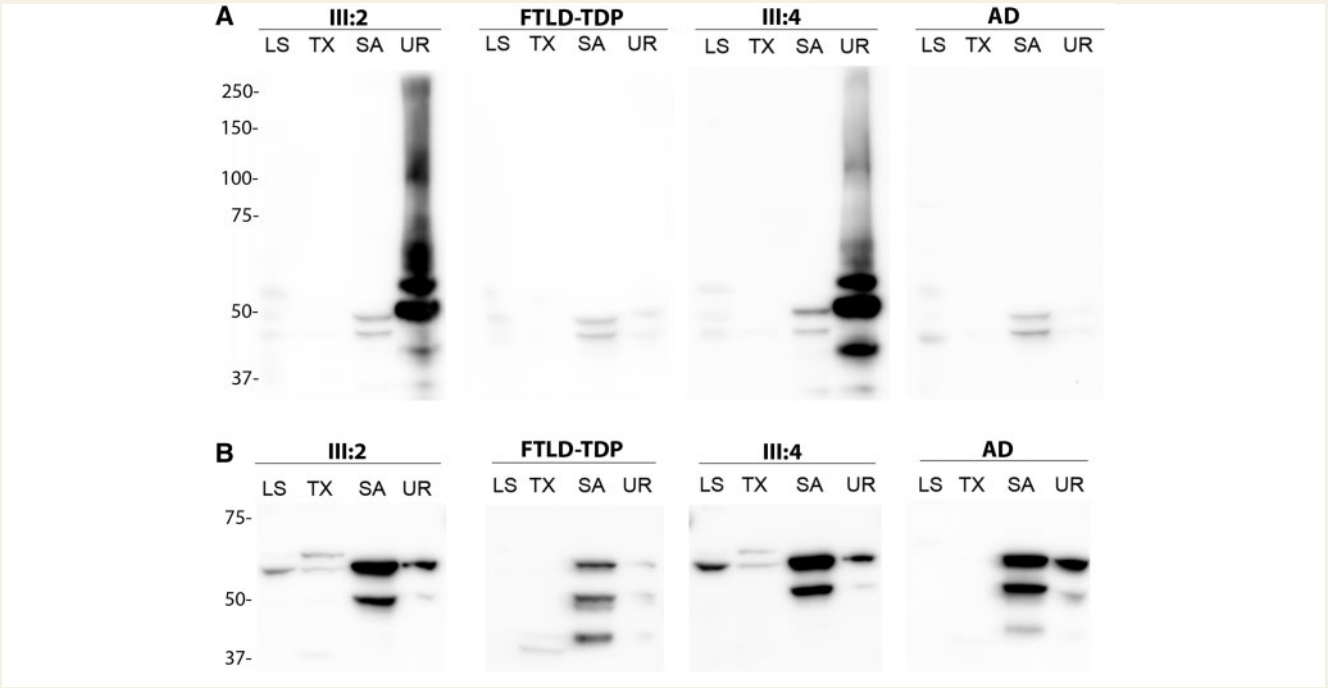

Figure 5 Biochemical analysis of PRKAR1B and α-internexin. (**A**) Proteins were sequentially extracted from temporal grey matter from two cases (Patients III:2 and III:4) with the *PRKAR1B* mutation and neurological controls [Alzheimer's disease (AD) and frontotemporal lobar degeneration with TARDBP inclusions (FTLD-TDP)]. Low salt (LS), Triton^{TM} X-100- (TX), sarkosyl (SA) and urea (UR) fractions were separated by SDS-PAGE and immunoblotted with anti-PKA RI antibody (BD Laboratories). Cases and controls showed bands in the sarkosyl fraction corresponding to PRKAR1A (~48 kDa) and PRKAR1B (~50 kDa). Note the dramatic increase of highly-insoluble PRKAR1B in the urea fraction in cases compared with controls accompanied by appearance of additional bands of ~45 kDa and ~55 kDa and a high molecular mass smear. (**B**) The same protein fractions were analysed by α-internexin immunoblot revealing no obvious changes with respect to changes in solubility or appearance of additional bands between cases and controls.

high relative molecular mass (M_r) smear. Similar results were observed with a second antibody raised against PRKAR1B (Santa Cruz, data not shown). As the appearance of higher migrating bands is suggestive for abnormal post-translational modifications such as hyperphosphorylation, we investigated the phosphorylation state of PRKAR1B by treating dialyzed urea fractions with lambda protein phosphatase. However, this did not reveal any obvious changes in the banding pattern (Supplementary Fig. 4). No biochemical alterations with respect to changes in solubility or appearance of additional bands were observed for α-internexin between our *PRKAR1B* mutation cases and controls (Fig. 5B).

In silico prediction of the *PRKAR1B* mutation on PRKAR1B protein structure

PRKAR1B codes for the R1β-subunit of cyclic AMP-dependent protein kinase A, which is a tetramer in its inactive form composed of two catalytic and two regulatory subunits (Fig. 6A and B) (Ilouz *et al.*, 2012). Binding of cyclic AMP to the regulatory subunits unleashes the catalytic subunits, thereby allowing phosphorylation of PKA substrates. The regulatory subunits dimerize through their N-terminal dimerization/docking (D/D) domains. In the inactive PKA tetramer, the D/D domains of the R1β isoform form an integral part of the holoenzyme; while the cyclic AMP binding domains and the linker region tightly interact with one catalytic subunit additional *trans* interactions with the catalytic subunit in the other heterodimer (Fig. 6B). The leucine at position 50 of the PRKAR1B protein is located on the dimer interface formed by the N-terminal D/D domains of the regulatory subunits (Fig. 6A). The leucine side chain forms a hydrophobic core together with several other conserved hydrophobic residues to create this dimer interface (Fig. 6B). A change of leucine to arginine at this position creates a steric hindrance, because of its larger size the arginine side chain will not fit within the hydrophobic core. Furthermore, the positive charge on the arginine side chain will potentially introduce unfavourable electrostatic interactions with its symmetry-related arginine across the dimer interface. In one scenario, the dimerization interface may still be formed but with local structural rearrangements resulting in an altered conformation. Due to the intimate connections between the D/D domains and the catalytic subunits, these local rearrangements may be propagated throughout the holoenzyme and affect the cyclic AMP-induced response and thus activation of the kinase (Ilouz *et al.*, 2012). Furthermore, the D/D dimerization interface creates the docking site for AKAPs (Fig. 6C) (Sarma *et al.*, 2010), and local rearrangements may affect AKAP binding and thereby PKA signalling and targeting PKA to a specific subcellular location

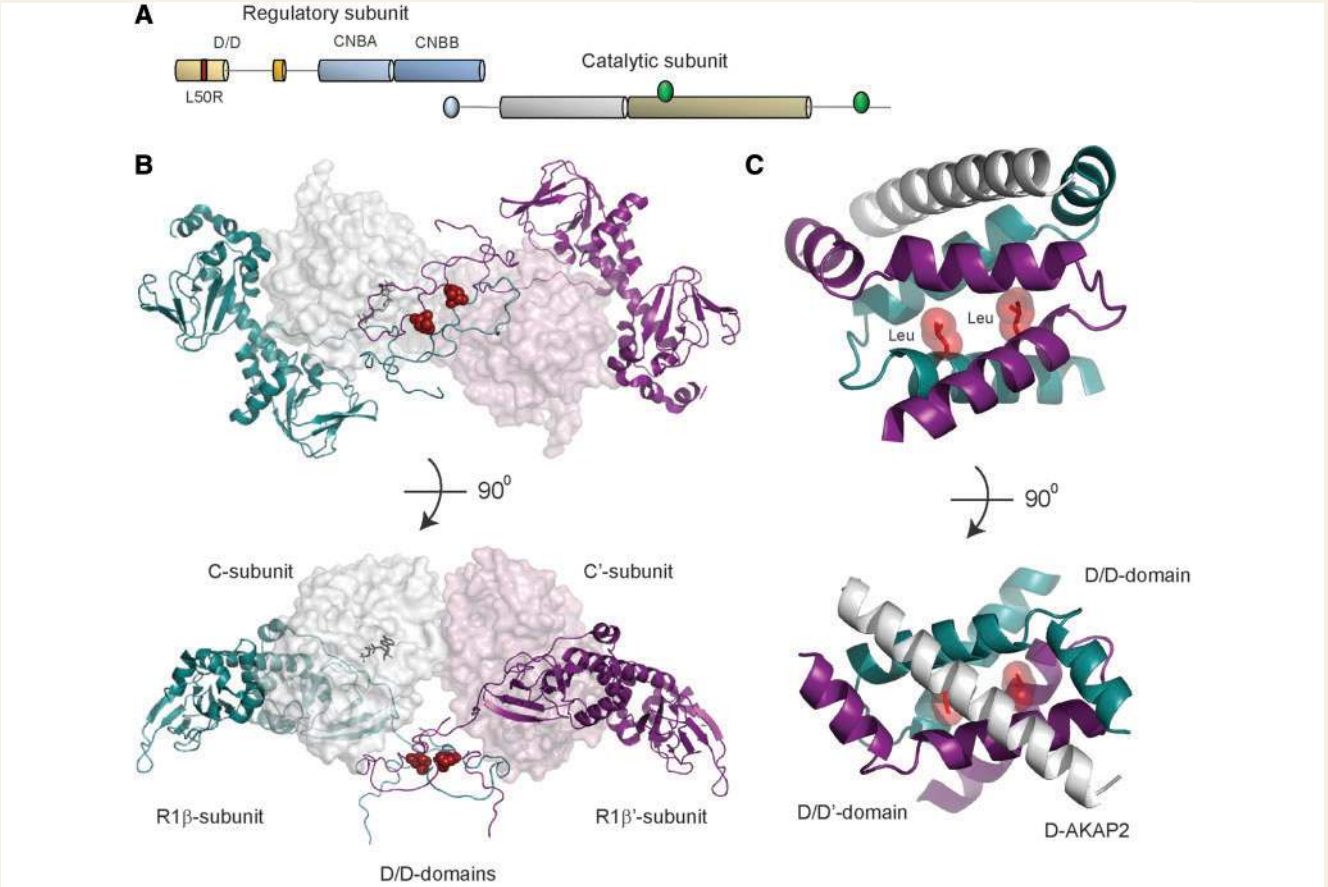

Figure 6 The L50R mutation is located on the interface between the docking/dimerization domains of the protein kinase A regulatory subunit β. (**A**) Organization of the PKA protein subunits. The regulatory subunits contain an N-terminal dimerization/docking (D/D) domain, followed by a linker region and two cAMP binding domains (CNBA and CNBB). The catalytic subunit contains an N-terminal myristylation site for membrane anchoring (blue circle), N-and C-terminal lobes and tails with phosphorylation sites (green circles). The p.Leu50Arg mutation maps to the D/D domain of the regulatory subunit. (**B**) Overall structure of the PKA tetrameric holoenzyme containing two catalytic and two regulatory subunits. The catalytic subunits C (white) and C′ (pink) are shown in space filling representation, with ATP bound to subunit C represented in black sticks. The secondary structure elements of the regulatory subunits are shown in cyan (subunit R1β = PRKAR1B) and in purple (symmetry-related subunit R1β′) with the leucine on the interface between the D/D domains in red space filling representation. The holoenzyme is shown in two different orientations. (**C**) The importance of the D/D-dimer interface formation for binding to A-kinase anchoring proteins is shown by the structure of the D/D domain of the homologous PRKAR1α subunit in complex with a peptide from Dual-specific AKAP2. Secondary structures are shown in cyan and purple (regulatory subunit D/D domains) and white (dual-specific AKAP2). Side chains of Leu50 at the D/D interface are indicated in red stick representation surrounded by transparent spheres. Figure is created using Pymol (deLano Scientific).

(Sarma *et al.*, 2010; Taylor *et al.*, 2012). In another scenario the arginine completely prevents formation of the dimerization interface between the D/D domains. This would affect correct holoenzyme formation and thereby PKA activation. In addition, the unassembled D/D domain interfaces would expose large hydrophobic areas which are prone to aggregation resulting in insoluble protein.

Discussion

This study describes a novel hereditary neurodegenerative disorder associated with a mutation (c.149T>G; p.Leu50Arg; RefSeq NM_002735.2, NP_002726.1) in the gene coding for the type I-beta regulatory subunit of the PKA with a unique neuropathological phenotype with PRKAR1B accumulation into abundant neuronal inclusions. The mutation is predicted to prevent or alter dimerization between the D/D domains within the PKA holoenzyme, thereby exposing hydrophobic protein regions that may result in aggregation, or reducing the binding of the regulatory subunits to both the catalytic subunits of PKA, and to AKAP. The frequency of this mutation appears to be rare, as the mutation is absence in dbSNP and Exome Variant Server. Moreover, no pathogenic mutation in *PRKAR1B* could be identified in a cohort of familial Parkinson's disease or frontotemporal dementia.

The present disorder has a rather unspecific phenotype consisting of dementia and parkinsonism with poor response to levodopa, normal FP-CIT scan, and normal CSF biomarkers, which

have ruled out Parkinson's disease and Alzheimer's disease. The neuropsychological profile with impairment of multiple cognitive domains and clinical symptoms are consistent with the involvement of all cortical and subcortical regions of the brain. Cerebellar and motor neuron signs were lacking at neurological examination despite the widespread inclusions in cerebellum and spinal cord; however, we cannot exclude that the patients may develop such signs in the last stage of the disease during their stay in a nursing home. Its hereditary occurrence has initially not been recognized (van Duinen *et al.*, 1999), but distinguishes it from the mostly sporadic NIFID. Furthermore, the absence of immunoreactivity with α-synuclein and FUS antibodies distinguishes this disorder from Parkinson's disease and NIFID. The co-occurrence with cancers (myeloid leukaemia and glioblastoma) in two of five patients is quite remarkable. PKA stimulates the expression of the NR4 receptor, and NR4 is involved in several malignancies, such as glioblastoma and myeloid leukaemia (Mohan *et al.*, 2012). It might be worth screening for potential variants in *PRKAR1B* in cohorts of patients with these malignancies and to see whether the mutation alters the expression of NR4 receptor. However, this is beyond the scope of this research.

The present approach of combining genome-wide linkage analysis, exome sequencing and proteomic analysis of neuronal inclusions allowed us to identify a heterozygous p.Leu50Arg variant in *PRKAR1B* in five affected family members, consistent with an autosomal dominant mode of inheritance. The highly specific pattern of PRKAR1B accumulation in inclusions in the three autopsy-proven cases together with the dramatic enrichment of PRKAR1B in highly insoluble protein fractions with appearance of abnormal M_r species, the negative PRKAR1B immunoreactivity in any other neurodegenerative disorders (Alzheimer's disease, Parkinson's disease, Lewy body dementia, multiple system atrophy, Pick's disease, and FTLD-TARDBP) and the absence of the mutation in variant databases, strongly argues for a causative role of this mutation in this family.

The pathophysiological mechanism by which this mutation leads to neurodegenerative disease remains to be investigated by establishing cell culture and animal models. Our first hypothesis is that the mutation leads to impaired dimerization between the regulatory R1β subunits and catalytic subunits within the PKA holoenzyme. Structural changes within the holoenzyme may liberate the catalytic subunits which could be vulnerable to degradation, resulting in reduced PKA activity. This hypothesis is supported by loss of PKA catalytic subunit and PKA activity shown in PKA regulatory knockout mice (Burton *et al.*, 1997). However, catalytic subunits unleashed by mutation-induced structural changes may also lead to increased PKA activity, as has been found in the p.Ser9Asn mutation of PRKAR1A (Greene *et al.*, 2008). PRKAR1B knock-out mice have impaired long-term potentiation and long-term depression in the mossy fibres—cornu ammonis 3 region of the hippocampus and visual cortex (Brandon *et al.*, 1995; Qi *et al.*, 1996; Hensch *et al.*, 1998).

A second pathophysiological mechanism is that the Leu50Arg mutation on the subunit interface of the D/D-domain can induce structural changes to the docking site for AKAP which is located across this interface, and abolish the binding between AKAP and the regulatory subunit (Sarma *et al.*, 2010; Ilouz *et al.*, 2012). An important function of AKAP is to target the holoenzyme in close proximity to the dedicated substrates by binding to the D/D-domain (Ilouz *et al.*, 2012), which is important for creating the microenvironment for PKA signalling. It is likely that impaired binding to AKAP causes subcellular dislocalization of the complex, thereby disturbing PKA signalling on the dedicated substrates.

The Leu50Arg *PRKAR1B* mutation and subsequent change in PKA function probably leads to an imbalance of the phosphorylation status of N-terminal head and C-terminal tail domain of neurofilaments. PKA is responsible for transient phosphorylation of specific sites on the N-terminal head domain of neurofilaments (Zheng *et al.*, 2003). Phosphorylation levels of N- and C-terminal are related to each other, and are essential for axonal transport (Zheng *et al.*, 2003; Dale and Garcia, 2012). Therefore, the imbalance of phosphorylation would explain the additional accumulation of α-internexin and other neurofilaments in the cell soma in the present cases.

The aggregate formation of PRKAR1B, its biochemical enrichment and additional bands in urea fractions can be the result of post-translational modifications such as (hyper)phosphorylation. Although our dephosphorylation experiments are not indicative of abnormal phosphorylation, more sophisticated biochemical analyses are needed to further address this. In addition, the high M_r smear in the immunoblot might be explained by poly-ubiquitination of PRKAR1B protein in the proteosomal degradation (Lignitto *et al.*, 2011). The aggregation of PRKAR1B might entrap other proteins like intermediate filaments just as a secondary phenomenon, as we see in inclusions characteristic for other neurodegenerative diseases (Szaro and Strong, 2010).

Although we have not seen obvious changes and presence of abnormal M_r α-internexin protein species in our cases by immunoblot, the analysis of phosphorylation alterations of intermediate filaments requires further investigation by more sensitive means such as mass spectrometry. Future studies to explore the phosphorylation of intermediate filaments in model systems carrying the Leu50Arg mutation are required to address this. Finally, the unique pathological phenotype of the present disorder is supported by the distinct pattern of PKA type I regulatory bands on western blots of brain tissue. To find out the reason of the different pattern between cases and controls, more sophisticated proteomic analysis would be required in the future.

In conclusion, we provide evidence that a mutation in *PRKAR1B* is associated with a new type of a familial neurodegenerative disease with dementia and parkinsonism characterized by specific and abundant accumulation of PRKAR1B into neuronal inclusions. Our findings link altered regulation of PKA by mutant PRKAR1B to human late-onset neurodegeneration.

Acknowledgements

We would like to thank Tom de Vries Lentsch and Ruud Koppenol for excellent photography, and J.G.J. van Rooij for the technical support of the exome sequencing. We are grateful to Prof. B.A. Oostra and Prof. P. Heutink for genetic advice, and T. Revesz for

discussing microscopy. We thank all the participating subjects for devoting their time, efforts, and collaboration.

Funding

This work was supported by grant from Hersenstichting Nederland (grant nr. 2012(1)-23), Internationale Stichting Alzheimer Onderzoek (grant nr. #11519) and Alzheimer Nederland (grant nr. WE.05-2010-06). A.B. Smit and K.W. Li, received support from EU-HEALTH-2009-2.1.2-1, SYNSYS project (grant nr. 242167), and from the Center of Medical Systems Biology (CMSB). V.B. received support from the Stichting Parkinson Fonds (The Netherlands).

Supplementary material

Supplementary material is available at *Brain* online.

References

Brandon EP, Zhuo M, Huang YY, Qi M, Gerhold KA, Burton KA, et al. Hippocampal long-term depression and depotentiation are defective in mice carrying a targeted disruption of the gene encoding the RI beta subunit of cAMP-dependent protein kinase. Proc Natl Acad Sci USA 1995; 92: 8851–5.

Burgers PP, Ma Y, Margarucci L, Mackey M, van der Heyden MA, Ellisman M, et al. A small novel A-kinase anchoring protein (AKAP) that localizes specifically protein kinase A-regulatory subunit I (PKA-RI) to the plasma membrane. J Biol Chem 2012; 287: 43789–97.

Burton KA, Johnson BD, Hausken ZE, Westenbroek RE, Idzerda RL, Scheuer T, et al. Type II regulatory subunits are not required for the anchoring-dependent modulation of Ca2+ channel activity by cAMP-dependent protein kinase. Proc Natl Acad Sci USA 1997; 94: 11067–72.

Cairns NJ, Grossman M, Arnold SE, Burn DJ, Jaros E, Perry RH, et al. Clinical and neuropathologic variation in neuronal intermediate filament inclusion disease. Neurology 2004a; 63: 1376–84.

Cairns NJ, Neumann M, Bigio EH, Holm IE, Troost D, Hatanpaa KJ, et al. TDP-43 in familial and sporadic frontotemporal lobar degeneration with ubiquitin inclusions. Am J Pathol 2007; 171: 227–40.

Cairns NJ, Uryu K, Bigio EH, Mackenzie IR, Gearing M, Duyckaerts C, et al. alpha-Internexin aggregates are abundant in neuronal intermediate filament inclusion disease (NIFID) but rare in other neurodegenerative diseases. Acta Neuropathol 2004b; 108: 213–23.

Cairns NJ, Zhukareva V, Uryu K, Zhang B, Bigio E, Mackenzie IR, et al. alpha-internexin is present in the pathological inclusions of neuronal intermediate filament inclusion disease. Am J Pathol 2004c; 164: 2153–61.

Chang A, Li PP, Warsh JJ. Altered cAMP-dependent protein kinase subunit immunolabeling in post-mortem brain from patients with bipolar affective disorder. J Neurochem 2003; 84: 781–91.

Ching GY, Chien CL, Flores R, Liem RK. Overexpression of alpha-internexin causes abnormal neurofilamentous accumulations and motor coordination deficits in transgenic mice. J Neurosci 1999; 19: 2974–86.

Dale JM, Garcia ML. Neurofilament phosphorylation during development and disease: which came first, the phosphorylation or the accumulation? J Amino Acids 2012; 2012: 382107.

Dequen F, Cairns NJ, Bigio EH, Julien JP. Gigaxonin mutation analysis in patients with NIFID. Neurobiol Aging 2011; 32: 1528–9.

Edgar RC. MUSCLE: multiple sequence alignment with high accuracy and high throughput. Nucleic Acids Res 2004; 32: 1792–7.

Fabrizi GM, Cavallaro T, Angiari C, Bertolasi L, Cabrini I, Ferrarini M, et al. Giant axon and neurofilament accumulation in Charcot-Marie-Tooth disease type 2E. Neurology 2004; 62: 1429–31.

Gibb BJ, Brion JP, Brownlees J, Anderton BH, Miller CC. Neuropathological abnormalities in transgenic mice harbouring a phosphorylation mutant neurofilament transgene. J Neurochem 1998; 70: 492–500.

Greene EL, Horvath AD, Nesterova M, Giatzakis C, Bossis I, Stratakis CA. *In vitro* functional studies of naturally occurring pathogenic PRKAR1A mutations that are not subject to nonsense mRNA decay. Hum Mutat 2008; 29: 633–9.

Gudbjartsson DF, Jonasson K, Frigge ML, Kong A. Allegro, a new computer program for multipoint linkage analysis. Nat Genet 2000; 25: 12–3.

Hensch TK, Gordon JA, Brandon EP, McKnight GS, Idzerda RL, Stryker MP. Comparison of plasticity *in vivo* and *in vitro* in the developing visual cortex of normal and protein kinase A RIbeta-deficient mice. J Neurosci 1998; 18: 2108–17.

Hoffmann K, Lindner TH. easyLINKAGE-Plus—automated linkage analyses using large-scale SNP data. Bioinformatics 2005; 21: 3565–7.

Holmgren A, Bouhy D, Timmerman V. Neurofilament phosphorylation and their proline-directed kinases in health and disease. J Peripher Nerv Syst 2012; 17: 365–76.

Hughes AJ, Daniel SE, Kilford L, Lees AJ. Accuracy of clinical diagnosis of idiopathic Parkinson's disease: a clinico-pathological study of 100 cases. J Neurol Neurosurg Psychiatry 1992; 55: 181–4.

Ilouz R, Bubis J, Wu J, Yim YY, Deal MS, Kornev AP, et al. Localization and quaternary structure of the PKA RIbeta holoenzyme. Proc Natl Acad Sci USA 2012; 109: 12443–8.

Josephs KA, Holton JL, Rossor MN, Braendgaard H, Ozawa T, Fox NC, et al. Neurofilament inclusion body disease: a new proteinopathy? Brain 2003; 126: 2291–303.

Lariviere RC, Julien JP. Functions of intermediate filaments in neuronal development and disease. J Neurobiol 2004; 58: 131–48.

Li H, Durbin R. Fast and accurate short read alignment with Burrows-Wheeler transform. Bioinformatics 2009; 25: 1754–60.

Lignitto L, Carlucci A, Sepe M, Stefan E, Cuomo O, Nistico R, et al. Control of PKA stability and signalling by the RING ligase praja2. Nat Cell Biol 2011; 13: 412–22.

McKenna A, Hanna M, Banks E, Sivachenko A, Cibulskis K, Kernytsky A, et al. The Genome Analysis Toolkit: a MapReduce framework for analyzing next-generation DNA sequencing data. Genome Res 2010; 20: 1297–303.

Mohan HM, Aherne CM, Rogers AC, Baird AW, Winter DC, Murphy EP. Molecular pathways: the role of NR4A orphan nuclear receptors in cancer. Clin Cancer Res 2012; 18: 3223–8.

Molina-Porcel L, Llado A, Rey MJ, Molinuevo JL, Martinez-Lage M, Esteve FX, et al. Clinical and pathological heterogeneity of neuronal intermediate filament inclusion disease. Arch Neurol 2008; 65: 272–5.

Momeni P, Cairns NJ, Perry RH, Bigio EH, Gearing M, Singleton AB, et al. Mutation analysis of patients with neuronal intermediate filament inclusion disease (NIFID). Neurobiol Aging 2006; 27: 778 e1–e6.

Neumann M, Roeber S, Kretzschmar HA, Rademakers R, Baker M, Mackenzie IR. Abundant FUS-immunoreactive pathology in neuronal intermediate filament inclusion disease. Acta Neuropathol 2009; 118: 605–16.

Neumann M, Sampathu DM, Kwong LK, Truax AC, Micsenyi MC, Chou TT, et al. Ubiquitinated TDP-43 in frontotemporal lobar degeneration and amyotrophic lateral sclerosis. Science 2006; 314: 130–3.

O'Connell JR, Weeks DE. PedCheck: a program for identification of genotype incompatibilities in linkage analysis. Am J Hum Genet 1998; 63: 259–66.

Qi M, Zhuo M, Skalhegg BS, Brandon EP, Kandel ER, McKnight GS, et al. Impaired hippocampal plasticity in mice lacking the Cbeta1 catalytic subunit of cAMP-dependent protein kinase. Proc Natl Acad Sci USA 1996; 93: 1571–6.

Rao MV, Yuan A, Campbell J, Kumar A, Nixon RA. The C-terminal domains of NF-H and NF-M subunits maintain axonal neurofilament content by blocking turnover of the stationary neurofilament network. PLoS One 2012; 7: e44320.

Sarma GN, Kinderman FS, Kim C, von Daake S, Chen L, Wang BC, et al. Structure of D-AKAP2:PKA RI complex: insights into AKAP specificity and selectivity. Structure 2010; 18: 155–66.

Sasaki T, Gotow T, Shiozaki M, Sakaue F, Saito T, Julien JP, et al. Aggregate formation and phosphorylation of neurofilament-L Pro22 Charcot-Marie-Tooth disease mutants. Hum Mol Genet 2006; 15: 943–52.

Sihag RK, Jaffe H, Nixon RA, Rong X. Serine-23 is a major protein kinase A phosphorylation site on the amino-terminal head domain of the middle molecular mass subunit of neurofilament proteins. J Neurochem 1999; 72: 491–9.

Skalhegg BS, Tasken K. Specificity in the cAMP/PKA signaling pathway. Differential expression,regulation, and subcellular localization of subunits of PKA. Front Biosci 2000; 5: D678–93.

Szaro BG, Strong MJ. Post-transcriptional control of neurofilaments: new roles in development, regeneration and neurodegenerative disease. Trends Neurosci 2010; 33: 27–37.

Taylor SS, Ilouz R, Zhang P, Kornev AP. Assembly of allosteric macromolecular switches: lessons from PKA. Nat Rev Mol Cell Biol 2012; 13: 646–58.

Uchikado H, Shaw G, Wang DS, Dickson DW. Screening for neurofilament inclusion disease using alpha-internexin immunohistochemistry. Neurology 2005; 64: 1658–9.

van Duinen SG, Lammers GJ, Maat-Schieman ML, Roos RA. Numerous and widespread alpha-synuclein-negative Lewy bodies in an asymptomatic patient. Acta Neuropathol 1999; 97: 533–9.

Wang K, Li M, Hakonarson H. ANNOVAR: functional annotation of genetic variants from high-throughput sequencing data. Nucleic Acids Res 2010; 38: e164.

Zhang L, Duan CJ, Binkley C, Li G, Uhler MD, Logsdon CD, et al. A transforming growth factor beta-induced Smad3/Smad4 complex directly activates protein kinase A. Mol Cell Biol 2004; 24: 2169–80.

Zheng YL, Li BS, Veeranna, Pant HC. Phosphorylation of the head domain of neurofilament protein (NF-M): a factor regulating topographic phosphorylation of NF-M tail domain KSP sites in neurons. J Biol Chem 2003; 278: 24026-32.

Appendix 1

Contributors from the International Parkinsonism Genetics Network

The Netherlands: V. Bonifati, G.J. Breedveld, Erasmus MC, Rotterdam; *Portugal*: J. Ferreira, L. Correia Guedes, Institute of Molecular Medicine, Lisbon; *Brazil*: H.F. Chien, E.R. Barbosa, University of São Paulo; *Italy*: A. Merola, M. Zibetti, L. Lopiano, University of Torino; C. Tassorelli, C. Pacchetti, G. Nappi, IRCCS Mondino, Pavia; G. Riboldazzi, G. Bono, Insubria University, Varese; A. Padovani, B. Borroni, University of Brescia; E. Fincati, L. Bertolasi, University of Verona; M. Tinazzi, A. Bonizzato, Borgo Trento Hospital, Verona; A. Dalla Libera, Boldrini Hospital, Thiene; P. Cortelli, S. Capellari, University of Bologna; M. Guidi, INRCA Institute, Ancona; P. Marini, F. Massaro, University of Firenze; R. Marconi, Misericordia Hospital, Grosseto; M. Onofrj, A. Thomas, University of Chieti-Pescara; N. Vanacore, National Institute of Health, Roma; G. Meco, G. Fabbrini, E. Fabrizio, M. Manfredi, A. Berardelli, Sapienza University, Roma; F. Stocchi, L. Vacca, IRCCS San Raffaele Pisana, Roma; M. De Mari, C. Dell'Aquila, Hospital of Andria; G. Iliceto, P. Lamberti, University of Bari; V. Toni, G. Trianni, Hospital of Casarano; V. Saddi, S. Francesco Hospital, Nuoro; G. Cossu, M. Melis, Hospital S. Michele AOB "G. Brotzu", Cagliari.